Evaluation of Eribulin Combined with Irinotecan for Treatment of Pediatric Cancer Xenografts

Andrew J. Robles[1], Raushan T. Kurmasheva[1], Abhik Bandyopadhyay[1], Doris A. Phelps[1], Stephen W. Erickson[2], Zhao Lai[1], Dias Kurmashev[1], Yidong Chen[1], Malcom A. Smith[3], and Peter J. Houghton[1]

ABSTRACT

Purpose: Vincristine combined with camptothecin derivatives showed synergy in preclinical pediatric cancer models, and the combinations are effective in treatment of childhood solid tumors. We determined whether the synergy between vincristine and irinotecan extends to eribulin, another microtubule inhibitor.

Experimental Design: Vincristine or eribulin, alone or combined with irinotecan, was studied in 12 xenograft models. Tumor regression and time to event were used to assess antitumor activity. Pharmacodynamic studies and RNA sequencing (RNA-seq) were conducted 24 and 144 hours after single-agent or combination treatment. Effects on vascular development were studied in Matrigel plugs implanted in mice. The interaction between binary combinations was examined *in vitro*.

Results: Eribulin combined with irinotecan was more effective than vincristine–irinotecan in 6 of 12 models. Pharmacodynamic markers induced by eribulin (phospho-histone H3) and irinotecan (γ-H2A.X) were abrogated in combination-treated tumors. The predominant RNA-seq signature in combination-treated tumors was activation of the TP53 pathway with increased nuclear TP53. Massive apoptosis was observed 24 hours only after treatment with the eribulin combination. *In vitro*, neither combination showed interaction using combination index analysis. Eribulin alone and the combination caused alterations in developing vasculature.

Conclusions: The eribulin combination is very active in these xenograft models, but not synergistic *in vitro*. The combination reduced pharmacodynamic markers indicative of single-agent mechanisms but in tumors, dramatically activated the TP53 pathway. Although a mechanism for *in vivo* synergy requires further study, it is possible that eribulin-induced inhibition of microtubule dynamics enhances irinotecan-induced nuclear accumulation of TP53, leading to rapid cell death.

Introduction

Current therapies for treatment of childhood cancers rely almost exclusively on use of cytotoxic agents, predominantly those that induce DNA damage, and antimitotic agents. Although the use of intensive chemotherapy has resulted in increased 5-year event-free survival (1, 2), and a high cure rate, the effects of chemoradiotherapy can be devastating (3–5). Development of new therapies for childhood solid tumors is slow and remains challenging. In part, this is because the number of drugs that can be tested is limited by a relatively low number of patients eligible for phase I/II evaluation. We and others have used pediatric patient-derived xenografts (PDX) and cell line-derived xenografts (CDX) to identify novel agents and effective combinations (6–11). These models were valuable in identifying combinations that were highly active in rhabdomyosarcoma, such as irinotecan–vincristine (9), and irinotecan–temozolomide (12) in other sarcomas (13). Several of these studies were confirmed in clinical trials (14, 15).

Camptothecin-based topisomerase I poisons have shown significant antitumor activity in multiple childhood xenograft models (6–8). Of note, both topotecan and irinotecan showed greater than additive activity when combined with vincristine (9, 10), and clinically, the combination of vincristine with irinotecan induces high objective response rates for advanced rhabdomyosarcoma (14), and anaplastic Wilms tumor (15). However, despite interesting preclinical activity and the clear demonstration of clinical utility of this combination, no mechanistic studies were undertaken to elucidate the basis for synergy.

Vincristine, a standard of care drug for many solid tumors and acute leukemias, binds tubulin and destabilizes microtubules, inhibiting mitotic progression. More recently, another microtubule inhibitor, eribulin, has shown impressive antitumor activity against a broad spectrum of cancer xenografts (16). Eribulin is a synthetic derivative of halichondrin B (17), that induces irreversible mitotic arrest. Eribulin prevents microtubule growth and suppresses dynamics by binding to their plus ends (18, 19). Eribulin may have activities in addition to its antimitotic effects; eribulin treatment has been reported to alter gene expression, induce tumor cell differentiation, cause vascular remodeling, reverse epithelial-to-mesenchymal transition (EMT), and inhibit Wnt/β-catenin signaling (16, 20–23). Eribulin demonstrated significant antitumor activity against sarcoma and acute lymphoblastic leukemia models (24), and it had far greater activity against Ewing sarcoma PDX models than vincristine (25). Eribulin has entered pediatric phase I testing (NCT02171260), with at least one partial response in a patient with Ewing sarcoma (26). Eribulin is approved for third-line therapy of breast cancer (27), and it was recently FDA approved for treatment of liposarcoma (28). Eribulin is also reported to

[1]Greehey Children's Cancer Research Institute, UT Health San Antonio, San Antonio, Texas. [2]RTI, Research Triangle Park, North Carolina. [3]Cancer Therapy Evaluation Program, National Cancer Institute, Bethesda, Maryland.

Note: Supplementary data for this article are available at Clinical Cancer Research Online (http://clincancerres.aacrjournals.org/).

A.J. Robles and R.T. Kurmasheva contributed equally to this article.

Corresponding Author: Peter J. Houghton, University of Texas Health Science Center at San Antonio, 8403 Floyd Curl Drive, Mail Code 7794, San Antonio, TX 78229. Phone: 210-562-9000; Fax: 210-567-6791; E-mail: HoughtonP@uthscsa.edu

Clin Cancer Res 2020;26:3012–23

doi: 10.1158/1078-0432.CCR-19-1822

Translational Relevance

Topoisomerase I poisons and microtubule-targeting agents, such as vincristine, are two of the most effective classes of chemotherapeutic agents used for the treatment of pediatric cancers. Recently, the microtubule inhibitor eribulin was approved for third-line treatment of breast cancer and liposarcoma. However, the efficacy of eribulin against pediatric solid tumors has not been thoroughly studied in the clinic. In this study, we evaluated the efficacy and mechanisms of action of eribulin and vincristine, alone and in combination with irinotecan, in preclinical xenograft models of pediatric solid tumors. Collectively, these studies provide rationale for further evaluation of eribulin alone, and eribulin combined with irinotecan for the treatment of pediatric solid tumors that are wild type for *TP53*.

have less neurotoxicity in preclinical models and patients (29, 30), and no peripheral neuropathy was observed in the phase I trial in children (26), suggesting eribulin may have advantages over vincristine with respect to long-term toxicity. In this study, we investigated the efficacy and mechanisms of action for eribulin and vincristine alone and in combination with irinotecan against pediatric PDX models.

Materials and Methods

Tumors and cell lines

PDXs (rhabdomyosarcomas Rh10, Rh30, Rh41, Rh65; Wilms tumor KT-11; and kidney rhabdoid tumor KT-14) and CDXs (Ewing sarcoma lines CHLA258, SK-NEP-1, ES-4) have been described previously (31). PDXs were established directly in mice without first being cultured *in vitro*, whereas CDXs were established from cell lines first grown in culture. RBD1 is an atypical teratoid rhabdoid tumor established from a metastatic lung lesion. All tumors were used at low passage and authenticated by STR analysis against reference profiles developed by this group.

Evaluation in xenograft models

C.B.17SC scid$^{-/-}$ (C.B-Igh-1b/*IcrTac-Prkdcscid*) female mice (Taconic Farms) were used to propagate subcutaneously implanted tumors as described previously (31). All mice were maintained under barrier conditions and experiments were carried out using protocols and conditions approved by the institutional animal care and use committee of UTHSA. Mice were randomized into groups of 10, and treatment was started when tumors were 200 to 400 mm^3. Methods similar to those developed in the Pediatric Preclinical Testing Program (PPTP) were used, only for these studies tumor volumes were measured for up to 20 weeks, and regrowth of tumors determined. Mice were evaluated weekly for tumor mass and body weight and endpoints were time to event, defined as tumor growing to 400% of its volume at the initiation of treatment, tumor regression [partial response (PR), ≥50% volume decrease; complete regression (CR), tumor volume <40 mm^3]. Eribulin was dissolved in sterile water and administered days 1 and 8, and irinotecan was dissolved in saline and administered days 1 to 5, with the cycle repeated at day 21. Eribulin was dosed at 1 mg/kg and irinotecan at 2.5 mg/kg. Both drugs were administered by intraperitoneal injection. Vincristine, as a single agent, was administered at 1 mg/kg every 7 days (intraperitoneally) for 6 consecutive weeks, or at 0.5 mg/kg when combined with irinotecan.

Statistical analyses

For combination testing, one objective was to determine whether the combination is significantly more effective than either agent utilized at their optimal/standard single-agent dose/schedule. This condition is termed therapeutic enhancement, which represents a therapeutic effect for which a tolerated regimen of a combination treatment exceeds the optimal effect achieved at any tolerated dose of monotherapy associated with the same drugs used in the combination (11, 32).

Evaluation of drug synergy

The cytotoxic activities of eribulin, vincristine, SN-38 (active metabolite of irinotecan), and the combinations were assessed by alamar blue assays (#BUF012; Bio-Rad Laboratories). ES-4 cells were plated in 96-well plates at 3.33×10^3 cells/well, allowed to adhere overnight, and treated with vehicle (0.5% DMSO) or drug for 72 hours. Alamar blue (10% culture volume) was added to each well and fluorescence was measured at 590 nm (excitation 570 nm). All samples were blank-corrected for the background fluorescence of alamar blue. Concentration–response curves were initially plotted and IC_{50} values were interpolated from nonlinear regressions using Prism 7 (Graphpad Software). Relevant concentration combinations of eribulin and SN-38 or vincristine and SN-38 were tested and combination indexes (CI) were calculated on the basis of the Bliss model of independence using the formula: $CI = (E_A + E_B - E_A E_B)/E_{AB}$, where ($E_A$, E_B) equal the effects of each individual drug and (E_{AB}) equals the effect of the drugs in combination. Heatmaps were produced using Prism 7. For the isobologram analysis, cells were treated with both drugs at fixed ratios. Concentration–response curves were generated at these fixed ratios and the IC_{50} values were determined. From these IC_{50} values, the concentrations of each individual drug at the IC_{50} were determined and plotted as an isobologram. CIs for these experiments were calculated on the basis of the Loewe additivity model using the formula $CI = a/A + b/B$, where (a, b) equal the concentrations of the combined drugs that produce a particular effect level and (A, B) equal the concentrations of each individual drug that produce the same effect level.

RNA sequencing library preparation and next-generation sequencing

Approximately 500 ng of total RNA from xenograft tissue was used for RNA sequencing (RNA-seq) library preparation by following the Illumina TruSeq stranded mRNA sample preparation guide (Illumina). RNA-seq libraries were subjected to quantification, and subsequent 50bp single-read sequencing module with Illumina HiSeq 3000 platform. After the sequencing run, demultiplexing with CASAVA (Illumina) was employed to generate the FastQ file for each sample. An average of ~35M reads were generated for each sample. All data are publicly available at the Gene Expression Omnibus (GEO) of the NCBI (GSE146687).

RNA-seq data analysis

All RNA-seq FastQ reads were aligned with the reference genome (UCSC human genome build hg19) using TopHat2 (33) default settings. The BAM files obtained after alignment were processed using HTSeq-count (34) to obtain the counts per gene in all samples. To remove RNA species from host (mouse RNA), a custom-designed algorithm was performed to align reads using TopHat2 to both host genome (mm9) and graft genome (hg19). We kept reads as human-specific or human/mouse-common based on number of mis-match bases, number of gaps, and alignment quality control scores. The

human RNA-seq reads were then re-aligned to graft genome hg19 using TopHat2 with default settings, and the BAM files obtained after alignment were processed using HTSeq-count to obtain the counts per gene. The R package DESeq (35) was used to normalize gene expression with the size factor method and perform pairwise comparisons between groups to identify differentially expressed genes (DEG). Genes with an FDR-adjusted P value <0.05 and at least a 2-fold change compared with control were considered to be significantly differentially expressed. Upon obtaining the DEGs from all pair-wise comparisons, we performed k-means clustering on the combined gene set ($k = 9$) with data ordered by untreated, eribulin (24 and 144 hours), irinotecan (24 and 144 hours), and combination (24 and 144 hours) using MATLAB (MathWorks). Additional quality control statistical analysis of outliers, intergroup variability, distribution levels, PCA, and hierarchical clustering analysis were performed to validate the experimental data. Pathway analysis was performed with ingenuity pathway analysis (IPA; Qiagen). Gene set enrichment analysis was performed with the software package distributed by the Broad Institute (36).

Immunoblotting

Snap frozen ES-4 and KT-11 tumors were ground under liquid N_2 and total protein extracted with cell lysis buffer (Cell Signaling Technology, #9803) containing Halt Protease Inhibitor Cocktail (Thermo Fisher Scientific) and 1 mmol/L phenylmethylsulfonylfluoride (Sigma-Aldrich). Protein concentrations of each lysate were measured with a Protein Assay Kit (Bio-Rad Laboratories) and 20 μg of total protein was separated on NuPAGE 4% to 12% or 10% Bis-Tris gels (Thermo Fisher Scientific). Proteins were transferred to Immobilon-FL PVDF membranes (MilliporeSigma) and probed with antibodies for cleaved PARP (Cell Signaling Technology, #5625), phospho-S139-H2A.X (#9718), TP53 (#48818), CDKN1A/p21 (#2947), MDM2 (#86934), PUMA/BBC3 (#12450), phospho-S345-Chk1 (#2348), Chk1 (#2360), phospho-T68-Chk2 (#2197), Chk2 (#3440), full length/cleaved caspase 3 (#9668), cleaved caspase 3 (#9664), phospho-S10-histone H3 (#53348), histone H3 (#4499), GAPDH (#2118), or RRM2B/p53R2 (Invitrogen, #PA5-19970). Primary antibodies were diluted in Odyssey Blocking Buffer (LI-COR) with 0.1% Tween 20 (Sigma-Aldrich). Membranes were incubated with IRDye 680 or IRDye 800CW-conjugated secondary antibodies (LI-COR) diluted in Odyssey Blocking Buffer with 0.1% Tween-20 and 0.01% SDS. Fluorescence was detected with an Odyssey CLx Imaging System and analyzed with Image Studio software (LI-COR).

IHC–chromogenic

Whole tumors were fixed overnight in PBS-buffered 10% formalin at 4°C, then transferred to 70% ethanol until processing. Tumors were embedded in paraffin, cut into 5-μm-thick sections, and mounted on positively-charged slides. Sections were deparaffinized with high-pH Target Retrieval Solution (Agilent) using a PT Link pretreatment module (Agilent) and stained for cleaved caspase 3 (Cell Signaling Technology, #9579), TP53 (Cell Signaling Technology, #48818), CD34 (Abcam, #ab81289), and alpha smooth muscle actin (α-SMA; Cell Signaling Technology, #19245) using a Dako Autostainer Link 48 (Agilent). Sections were counterstained with hematoxylin and visualized using an EnVision FLEX DAB+ sub-chromo dye system. Images were captured on an EasyScan digital slide scanner (Motic) at 40× magnification.

IHC–fluorescence

Tumors were snap frozen, embedded in O.C.T. compound (Scigen Inc., #4583), cut into 5 μm sections, and mounted on positively-charged slides. Immediately before immunostaining the O.C.T. sections were fixed with 4% paraformaldehyde (Santa Cruz Biotechnology, #281692) at room temperature and washed three times with PBS. Sections were blocked with 5% goat serum (Cell Signaling Technology, #5425), 0.3% Triton X-100 in PBS. Slides were incubated with primary antibodies diluted in 1% BSA, 0.3% Triton X-100 in PBS, overnight at 4°C in a humidified chamber. Primary antibodies were 53BP1 (Cell Signaling Technology, #4937), phospho-S10-H3 (#53348), or γ-H2A.X (Abcam, #ab26350). Sections were incubated with Alexa Fluor-488 or Alexa Fluor-647-conjugated secondary antibodies (Abcam, #ab150077 and #ab150115,) diluted in 1% BSA, 0.3% Triton X-100 in PBS. Slides were mounted with Prolong Gold Antifade Reagent with DAPI (Cell Signaling Technology, #8961) and 0.17-mm-thick cover glass. Images were captured with a FLUOVIEW FV3000 laser-scanning confocal microscope and analyzed with Fluoview software (Olympus).

Vascular development assays

C.B.17SC scid$^{-/-}$ female mice were implanted subcutaneously with 300 μL VEGF-infused (100 ng/mL) Matrigel, bilaterally into each flank. After 7 days, mice were assigned to four groups and left untreated (control) or treated with one cycle of eribulin, irinotecan, or the combination. One-hundred forty-four hours after the first drug dose (day 13 overall), mice were euthanized and plugs were excised, fixed in PBS-buffered 10% formalin containing 0.25% glutaraldehyde, and processed for IHC. Sections were stained for CD34 (Abcam) and α-SMA (Cell Signaling Technology). Immunostaining was quantified using FIJI software.

Results

In vivo evaluation of eribulin, vincristine, and irinotecan

Eribulin, vincristine, irinotecan, and the combinations were tested against 12 xenograft models (nine PDX, three CDX). With one exception (Rh10 treated with vincristine, $P = 0.322$), all treatments resulted in statistically significant increases in event-free survival (EFS) compared with controls ($P < 0.001$). Results are summarized in Supplementary Table S1, along with estimates of therapeutic enhancement, additivity, and *TP53* genotype. Details of the numbers of mice used, numbers that had events, or were excluded are given in Supplementary Table S2. Eribulin was administered at 1 mg/kg, which gives drug exposure in mice similar to that achieved after administration of 1.4 mg/m^2 to patients (24, 37). Eribulin induced regressions in nine models, with five PR, defined as ≥50% decrease in tumor volume, and four CR, defined as tumor volume <40 mm^3. These results are consistent with previous testing by PPTP, in which more intense treatment was administered (6). Irinotecan, administered at a dose and schedule that results in SN-38 (active metabolite of irinotecan) exposure similar to 50 mg/m^2 administered once daily for 5 days in children (38), induced tumor regressions in seven models, with one PR and six CR (Supplementary Tables S1 and S2).

Combining eribulin with irinotecan resulted in complete tumor regressions in five models, whereas in these models the best response for either single drug was PR. The addition of eribulin to irinotecan significantly prolonged time to event in each model tested. In ES-4 Ewing sarcoma xenografts, eribulin and irinotecan as single agents modestly reduced tumor growth (<50% growth inhibition), with increased time to event compared with control tumors of 8.4 and 9.1 days, respectively. In contrast, the combination induced CR in ES-4 xenografts, with EFS(T-C) of 62.9 days and met criteria for supra-additivity. Eribulin was more active against two other Ewing sarcoma

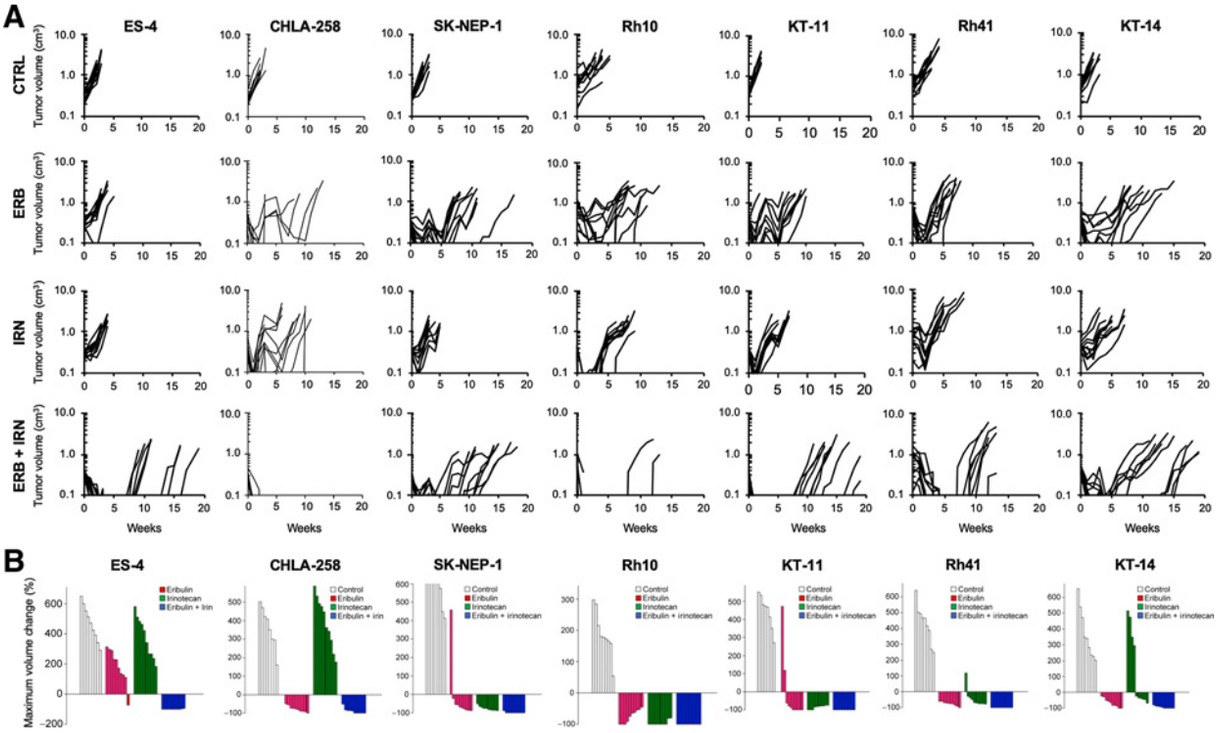

Figure 1.

Eribulin combined with irinotecan is more efficacious than either drug alone. Tumor-bearing mice were treated with eribulin (1 mg/kg days 1, 8, 21, 28) or irinotecan 2.5 mg/kg (days 1–5, 21–25), or the combination. **A,** Tumor growth curves for individual tumors in control mice (no treatment), eribulin treatment, irinotecan treatment, or combination treatment (top to bottom) in ES-4, CHLA258, SK-NEP-1, Rh10, KT-11, Rh41, and KT-14 xenografts. **B,** Waterfall plots showing the range of tumor growth or regression for individual tumors in each drug or combination group for ES-4, CHLA258, SK-NEP-1, Rh10, KT-11, Rh41, and KT-14 xenografts. ERB, eribulin; IRN, irinotecan; ERB+IRN, combination treatment.

xenografts, CHLA-258 (PR) and SK-NEP-1 (CR), with EFS(T-C) of 49.3 and 67.1 days, respectively (**Fig. 1**; Supplementary Table S1). Irinotecan induced PR in SK-NEP-1 xenografts but had little activity against CHLA-258 [<50% growth inhibition, EFS(T-C) of 7.1 days], whereas the combination induced CR in both CHLA-258 and SK-NEP-1, with EFS(T-C) of 81.6 and >120 days, respectively. EFS(T-C) for the combination treatment was additive for the individual agents in CHLA-258, but could not be estimated for SK-NEP-1 and KT-11 models as the median time to event exceeded the observation period. Similarly, using the EFS(T-C) metric, the combination effect could not be estimated for Rh10, Rh28, and Rh65 rhabdomyosarcoma models, but was additive in Rh30 and supra-additive in Rh41 models (Supplementary Table S1). However, the combination induced prolonged complete regressions in Rh10, Rh41, KT-11, and KT-14 (**Fig. 1**). Statistical analysis of therapeutic enhancement and additivity for the eribulin-irinotecan combination are presented in Supplementary Tables S1 and S3.

Vincristine was administered at 1 mg/kg, a dose that achieves plasma systemic exposures consistent with those seen in children administered 1.5 mg/m^2 (10, 39). In combination with irinotecan, the dose of vincristine had to be reduced to 0.5 mg/kg due to excessive toxicity. However, even with the dose reduction, the combination met criteria for therapeutic enhancement (i.e., significantly more activity for the combination than either single drug) and for supra-additivity in two models, SK-NEP-1 and ES-4 (Supplementary Table S4). The combination had significantly superior antitumor activity compared with vincristine at its MTD (1 mg/kg), against six models, and significantly superior activity compared with irinotecan alone in 10 of 12 models, the exceptions being KT-11 and Rh65. The combination of reduced dose vincristine with irinotecan was less active than vincristine (1 mg/kg dose) against KT-11 Wilms tumor. Of note, in xenograft models for which the combination of eribulin-irinotecan was superior to the combination of vincristine-irinotecan, all four models are *TP53* wild type, whereas the models for which the combinations had similar activity are predominantly *TP53* mutant (Supplementary Table S1).

Pharmacodynamic markers of drug action

Pharmacodynamic studies were conducted on tumors from 3 mice per group and focused on ES-4 (**Fig. 2**) and KT-11 (Supplementary Fig. S1), models in which we observed more than additive activity for the combination. Tumors were harvested 24 hours after the first drug administration to determine acute drug effects, and at 144 hours (24 hours after the final irinotecan treatment) to determine pharmacodynamic changes that associated with tumor response. In ES-4 xenografts, eribulin induced a robust increase in histone H3 phosphorylation at 24 hours (**Fig. 2A**), indicative of mitotic accumulation (40). Phospho-H3 was maintained at 144 hours, consistent with the high affinity of eribulin for microtubules and slow rate of release (41). In contrast, phospho-H3 had decreased to control levels at 144 hours after vincristine treatment (Supplementary Fig. S2A). Irinotecan slightly increased S139 phosphorylation of H2A.X (γ-H2A.X) at 24 hours, but induced a robust increase 24 hours after the fifth drug dose (144 hours), consistent with induction of DNA

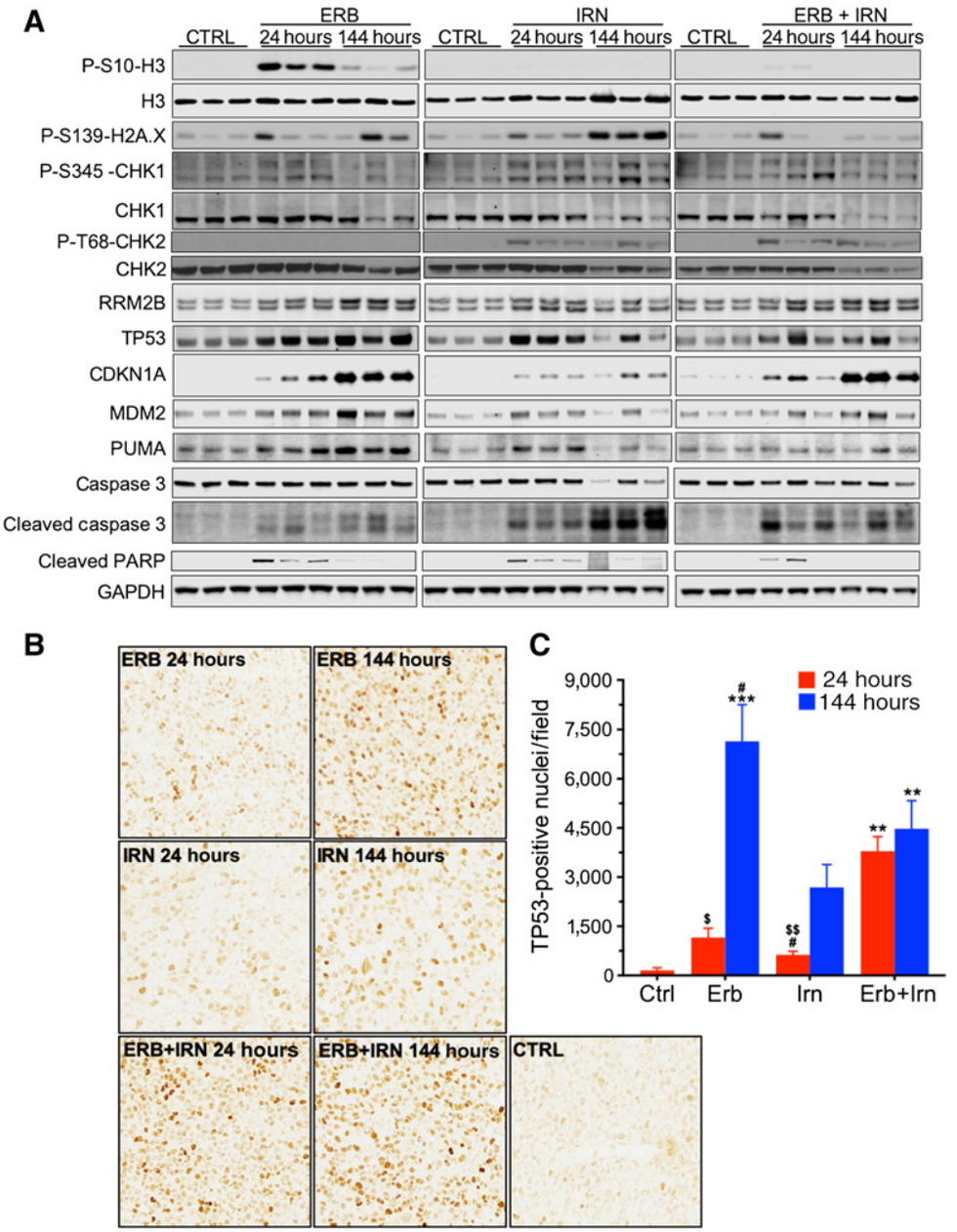

Figure 2.

Pharmacodynamic analysis of eribulin, irinotecan, and the combination in ES-4 xenografts. **A,** Immunoblotting of three independent ES-4 tumor lysates for markers of mitotic arrest (P-S10-histone H3), DNA damage (P-S139-H2A.X; P-S345-Chk1; P-T68-Chk2; RRM2B, ribonucleotide reductase regulatory TP53-inducible subunit M2B), TP53-regulated genes (TP53; cyclin-dependent kinase inhibitor 1A, p21; MDM2; PUMA), and apoptosis (full-length and cleaved caspase 3; cleaved PARP). GAPDH was used as a loading control. **B,** IHC for TP53 in ES-4 xenografts treated with eribulin, irinotecan, or the combination. Tumors were excised and processed at 24 and 144 hours after the first drug dose. **C,** Quantification of TP53 staining in ES-4 xenografts. *, $P < 0.033$, **, $P < 0.002$, ***, $P < 0.001$ compared with control; $^{\#}$, $P < 0.033$ compared with eribulin + irinotecan at 24 hours; $^{\$}$, $P < 0.033$, $^{\$\$}$, $P < 0.002$ compared with eribulin + irinotecan at 144 hours, two-way ANOVA with Tukey *post hoc* test. ERB, eribulin; IRN, irinotecan; ERB+IRN, combination treatment.

damage. Of note, both the eribulin-induced increase in phospho-H3 and the irinotecan-induced increase in γ-H2A.X were diminished in tumors from combination-treated mice (**Fig. 2**; Supplementary Figs. S1A and S3). In contrast, irinotecan effects on total and phosphorylated CHK1 and CHK2 proteins were similar in combination treated tumors. Thus, from a mechanism-based marker analysis, the combination would be considered as antagonistic, with apparently less eribulin-induced mitotic blockade and less DNA damage induced by irinotecan. Similar antagonism of phospho-H3 by irinotecan was observed in KT-11 xenografts (Supplementary Fig. S1A), although at

24 hours the induction of γ-H2A.X appeared to be greater in combination-treated tumors than in those from irinotecan-treated mice. Similar to the interaction between eribulin and irinotecan, the combination with vincristine resulted in diminished phospho-H3 at 24 hours and γ-H2A.X at 144 hours in ES-4 xenografts (Supplementary Fig. S2). These data suggest the S-phase arrest induced by irinotecan prevents eribulin- and vincristine-induced mitotic arrest.

We further investigated induction of DNA damage by eribulin, irinotecan, and the combination in ES-4 tumors by measuring 53BP1 and γ-H2A.X foci formation by immunofluorescence microscopy. At 144 hours, robust nuclear γ-H2A.X staining was observed following irinotecan treatment, but less intense staining was observed in the eribulin and combination-treated samples (Supplementary Fig. S4). In contrast, greater 53BP1 staining was observed in combination-treated tumors than in those treated with either single-agent. These data suggest the combination treatment resulted in more DNA double strand break formation than treatment with either single agent.

Induction of apoptosis

In ES-4 tumors, both eribulin and irinotecan alone induced modest PARP cleavage at 24 hours, whereas at 144 hours only tumors from irinotecan-treated mice showed detectable levels of cleaved PARP (**Fig. 2A**). For the eribulin–irinotecan combination, results were variable with detectable levels of cleaved PARP at 24 hours, but no cleaved PARP was detectable at 144 hours. In KT-11, eribulin alone induced modest PARP cleavage in tumors at 24 and 144 hours (Supplementary Fig. S1A). Irinotecan treatment resulted in robust PARP cleavage only at 24 hours in tumors (Supplementary Fig. S1A). For the combination, robust PARP cleavage was detected in two-third tumors at 24 hours and one-third tumors at 144 hours (Supplementary Fig. S1A). Abundance of cleaved caspase 3 was also evaluated by immunoblotting and IHC. Irinotecan induced caspase 3 cleavage at 24 hours and this increased at 144 hours in ES-4 xenografts (**Fig. 2A**). Cleaved caspase 3 was lower at 144 hours in tumors from combination treated mice (**Fig. 2A**). In KT-11 xenografts, cleaved caspase 3 was detected by immunoblot at both 24 and 144 hours only after irinotecan treatment (Supplementary Fig. S1A). By IHC staining, there was a significant increase at 24 hours in ES-4 and KT-11 tumors from combination treated mice compared with those receiving single-agent treatments (Supplementary Fig. S5). Collectively, these results indicate the combination treatment resulted in more apoptosis compared with either single-agent treatment.

Changes in gene expression

To further probe the mechanisms underlying the enhanced activity of the combination, gene expression was analyzed by RNA-seq in ES-4 tumors. Total reads and initial mapping rates for individual replicates are summarized in Supplementary Table S5 and the numbers of DEGs are summarized in Supplementary Table S6. At 24 hours, we identified 38, 896, and 984 DEGs (adjusted P value <0.05 and fold-change ≥2) in the eribulin, irinotecan, and combination groups, respectively. At 144 hours, 163, 1,759, and 2,114 genes were differentially expressed in these groups (adjusted P value <0.05 and fold-change ≥2). Some of the most significantly upregulated genes at 24 hours after eribulin treatment were hydroxyprostaglandin dehydrogenase 15-(NAD) (*HPGD*), chromosome 12 open reading frame 5 (*C12orf5*), cyclin-dependent kinase inhibitor 1A (*CDKN1A*/p21), tumor protein p53 inducible nuclear protein 1 (*TP53INP1*), pleckstrin homology-like domain, family A, member 3 (*PHLDA3*), BCL2 binding component 3 (*BBC3*; PUMA), and 15 histone encoding genes. At 144 hours, these genes remained elevated and MDM2 mRNA was found to be significantly increased as well. The upregulation of p21 and MDM2 mRNA after eribulin treatment was consistent with the increased protein levels observed by immunoblotting (**Fig. 2A**).

Similar to eribulin treatment, irinotecan induced TP53 responsive genes. Some of the most significantly upregulated genes after 24 hours of treatment included *SESN1, SESN2, MDM2, TP53AIP1, TPINIP1, RRM2B (*p53R2*), CDKN1A* (p21), and *BBC3* (PUMA; Supplementary Table S7), all of which remained upregulated at 144 hours. We collected all DEGs (n = 2,668) and performed k-means clustering analysis ($k = 9$). Among nine clusters, clusters 1, 3, and 8 (total of 1,615 genes) showed increased response in irinotecan or combination treated tumors (cluster 1, 804 genes; **Fig. 3A**, left). Overrepresentation enrichment analysis with enrichr (42) indicated "direct p53 effectors" as its main enrichment ($q = 1.97 \times 10^{-11}$). IPA further confirmed TP53 signaling functions ($P = 1.1 \times 10^{-11}$, **Fig. 3B**). The effect of combination treatment was additive in terms of increased expression compared with single-agent treatments for *TP53INIP1, RRM2B, CDKN1A*, and *MDM2* (Supplementary Table S7). Two exceptions were *BBC3*, which at 144 hours was similar to the irinotecan sample, and *TP53AIP1*, which was greater than the sum of the expression in tumors treated with single agents.

Activation of the TP53 pathway

The *TP53* status for each of the tumor models, where known, is included in Supplementary Table S1. Of the eight models where eribulin–irinotecan induced therapeutic enhancement, five lines have wild-type *TP53*, two have mutations, and the status of RBD1 is not determined. All four models where eribulin–irinotecan was dramatically more active than the vincristine–irinotecan combination are *TP53* wild type (defined as $EFS_{ERB/IRN}/EFS_{VCR/IRN}$ >1.5; range >1.53–4.22). Tumor samples were probed for activation of the TP53 pathway (TP53, MDM2, p21) by immunoblotting. In ES-4 tumors, eribulin treatment induced a robust increase in TP53 that was greatest at 144 hours, paralleled by increases in CDKN1A/p21 and MDM2 (**Fig. 2A**). The response to irinotecan was less pronounced, with an increase in TP53 at 24 hours which diminished at 144 hours. In tumors treated with the eribulin-irinotecan combination, TP53 and MDM2 levels were slightly lower than in the eribulin-treated tumors at 144 hours. However, the p21 levels were similar to those in the eribulin-treated tumors at both time points (**Fig. 2A**). Of note, in ES-4 tumors the TP53-regulated subunit of ribonucleotide reductase, RRM2B/p53R2, was upregulated by both eribulin and irinotecan, and the response at 144 hours to the combination was more similar to that induced by eribulin. The responses were more variable in KT-11 xenografts (Supplementary Fig. S1A); TP53 and p21 levels increased with each treatment at 24 hours, but the effects were diminished by 144 hours in all treatment groups.

We further evaluated induction of TP53 protein in ES-4 and KT-11 tumors by IHC (**Fig. 2B** and **C**; Supplementary Figs. S1B and S1C). In ES-4 tumors, single-agent treatment with eribulin resulted in a slight increase in nuclear TP53 staining at 24 hours, but a robust increase at 144 hours, compared with control (**Fig. 2B** and **C**). With irinotecan treatment, small but statistically insignificant increases in TP53 staining were observed at 24 and 144 hours. In contrast, the combination of eribulin and irinotecan resulted in significant increases in nuclear TP53 staining at both 24 and 144 hours (**Fig. 2B** and **C**), although this increase was less than that observed with eribulin alone at 144 hours.

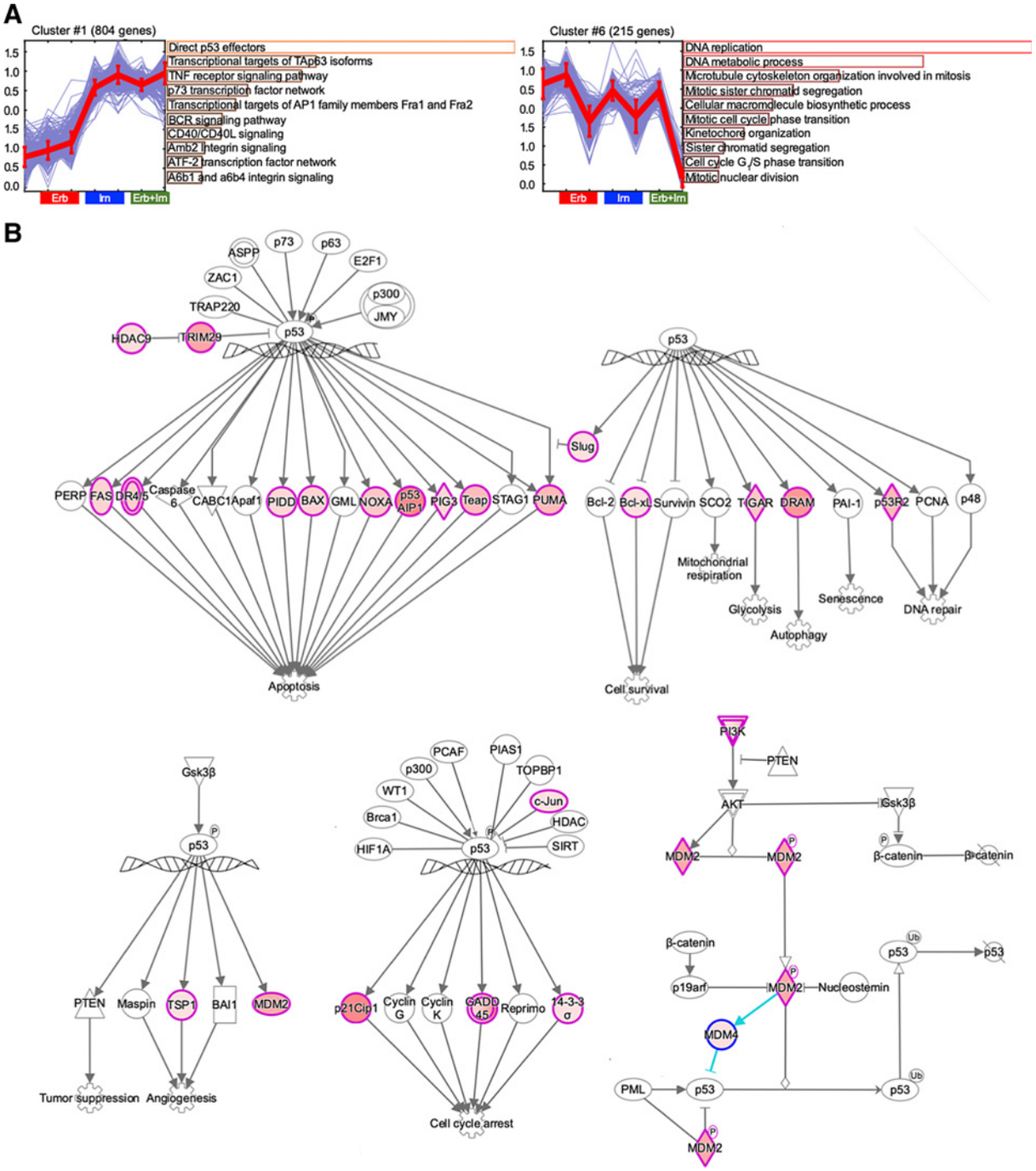

Figure 3.

Eribulin combined with irinotecan inhibits DNA replication and induces TP53 pathway genes. **A,** Clustering analysis of RNA-seq data (ES-4 xenografts) and trends over time for DNA replication and direct p53 effector gene clusters for each treatment group. **B,** IPA for TP53-related genes after combination treatment. Red color indicates significant upregulation of the gene relative to control samples.

TP53 staining in KT-11 xenografts showed rapid accumulation after 24 hours following eribulin, relatively little induction by irinotecan, but a dramatic increase in nuclear TP53 staining in tumors treated with the combination at 24 hours (Supplementary Figs. S1B and S1C). Nuclear TP53 was elevated at 144 hours in irinotecan treated KT-11 tumors, but had decreased in those from eribulin or combination treated tumors (Supplementary Figs. S1B and S1C). These results suggest the combination of eribulin–irinotecan results in a more rapid induction of the TP53 pathway than that occurring following single-agent treatment.

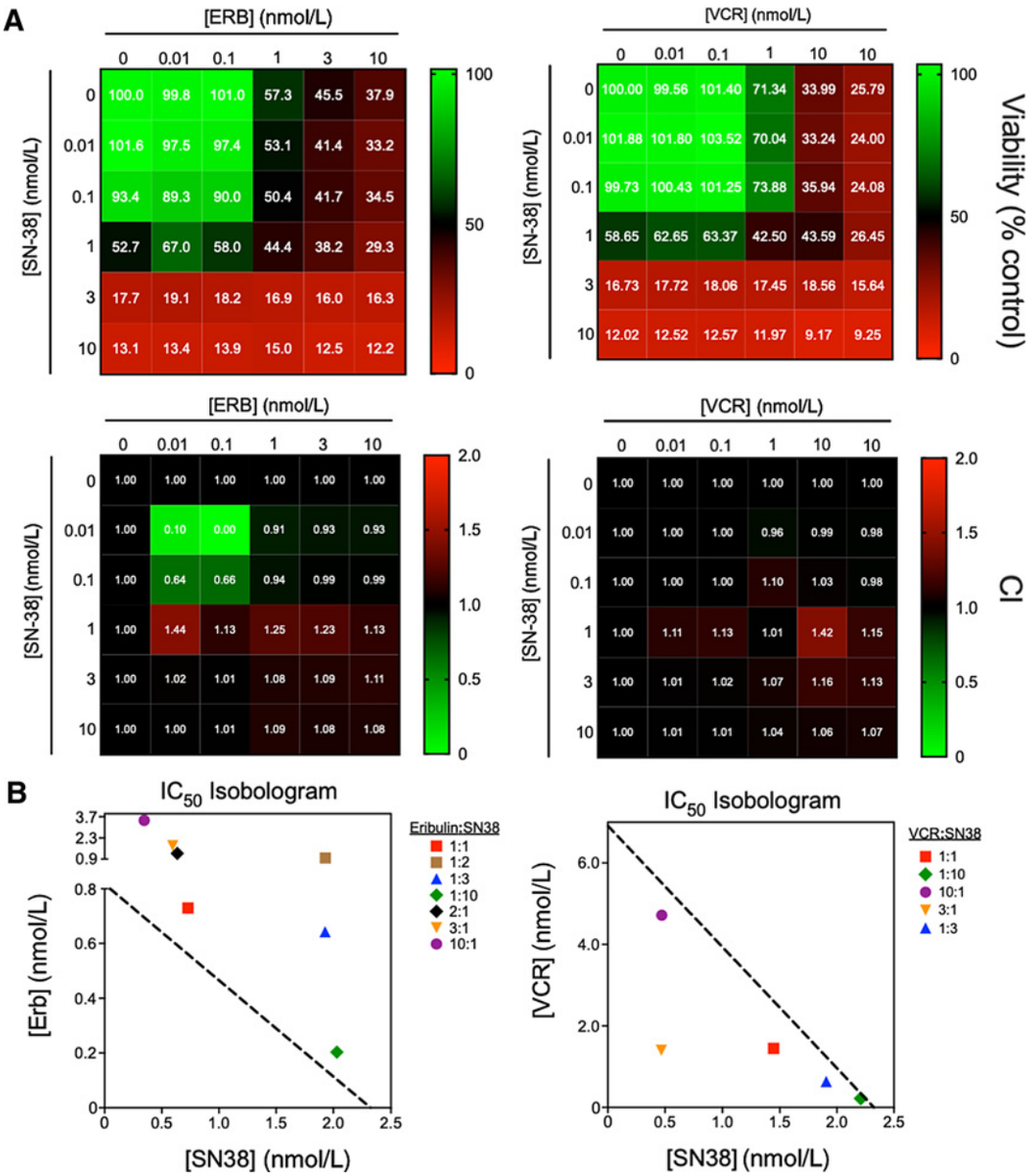

Figure 4.

Evaluation of drug combinations *in vitro*. **A,** Combination matrix heat maps for eribulin (ERB) or vincristine (VCR) combined with SN-38. Viability was measured using an alamarBlue assay, and CIs were calculated on the basis of the Bliss independence model. **B,** Isobolograms (50% effect level) for eribulin combined with SN-38 and vincristine combined with SN-38 in ES-4 cells; mean ± SE; $n \geq 3$ independent experiments.

In vitro evaluation of eribulin and SN-38

The antitumor activity of the eribulin–irinotecan combination was dramatic in some tumor models, yet the biomarkers reporting individual drug actions were muted in tumors treated with this combination relative to tumors from mice that received single agents. To resolve this discordance and further interrogate potential mechanism (s) by which the combination was synergistic *in vivo*, the *in vitro* cytotoxic effects of eribulin or vincristine combined with SN-38 were examined. All three drugs showed potent cytotoxic activity against ES-4 cells as single agents (**Fig. 4A**). The absolute IC_{50} values for eribulin, vincristine, and SN-38 were found to be 0.82, 6.9, and 2.3 nmol/L, respectively. CIs were calculated for multiple combination pairs of eribulin + SN-38 and vincristine + SN-38 based on the Bliss model of independence (**Fig. 4A**). For eribulin + SN-38, CIs were close to 1 at most concentration pairs, indicating additivity. CIs less than 1 were observed with combinations of relatively low concentration of each drug (0.01–0.1 nmol/L), suggesting synergy, but the effect sizes were very small (**Fig. 4A**). Similar results were observed with combinations of vincristine and SN-38, with most CIs indicating simple additive effects (**Fig. 4A**). To further assess the combined effects of eribulin or vincristine and SN-38, ES-4 cells were treated with both drugs at fixed ratios of eribulin:SN-38 and vincristine:SN-38. Isobologram

analysis showed that combination effects fell above the line of additivity suggesting that eribulin and SN-38 are antagonistic in terms of cytotoxic efficacy (**Fig. 4B**). CIs were calculated on the basis of the Loewe model of additivity for each fixed ratio and ranged from 1.12 to 4.38 (Supplementary Table S8). To determine if this antagonism was common among microtubule destabilizers, we assessed the *in vitro* interaction of vincristine and SN-38. In contrast to the antagonism seen with eribulin, most data points for vincristine and SN-38 fell close to or below the "line of additivity" at fixed ratios of vincristine:SN-38, indicating additivity or synergy with these combinations (**Fig. 4B**). CIs for these combinations ranged from 0.40 to 0.98 (Supplementary Table S8). Collectively, these results indicate that *in vitro* eribulin and vincristine have different effects, possibly linked to their different mechanisms of action, when combined with SN-38. However, studies in additional cell lines would be required to further establish this.

Effects of eribulin and irinotecan on tumor-dependent and tumor-independent vasculature

Eribulin has been shown to increase microvessel density and vascular permeability, which could increase drug uptake (43). To determine if eribulin, irinotecan, or the combination affects tumor vasculature, ES-4 tumor sections were stained for CD34 and α-SMA. There was a trend towards increased $CD34^{+}$ cells in tumors from combination-treated mice compared with control mice, although this was not statistically significant (**Figs. 5A** and **B**). Image quantification showed a nearly 6-fold increase in α-SMA-positive cells in combination-treated tumors compared with control tumors at 144 hours (**Fig. 5A** and **B**), suggesting an increase in tumor vasculature. We also assessed the effects of vincristine and vincristine combined with irinotecan on ES-4 tumor vasculature. We observed a decrease in CD34 staining after treatment with vincristine for 24 and 144 hours. Decreased CD34 staining was

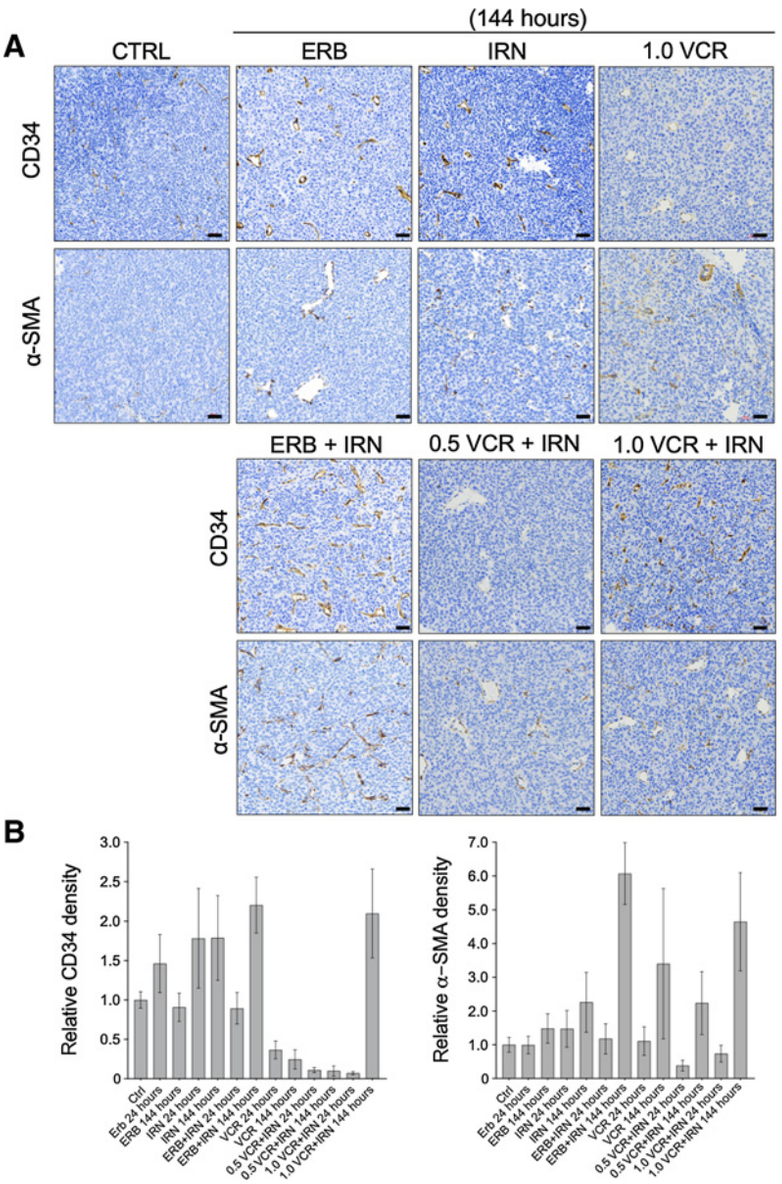

Figure 5.
Eribulin combined with irinotecan modifies tumor vasculature. **A,** IHC for CD34 and α-SMA in ES-4 xenografts after 144 hours treatment with single agents (top panels) or eribulin + irinotecan or vincristine + irinotecan. Black scale bars = 60 μm. **B,** Quantification of IHC staining for three tumor sections per treatment group (24 and 144 hours). Data represent mean ± SE; $n = 3$ independent tumor sections per group.

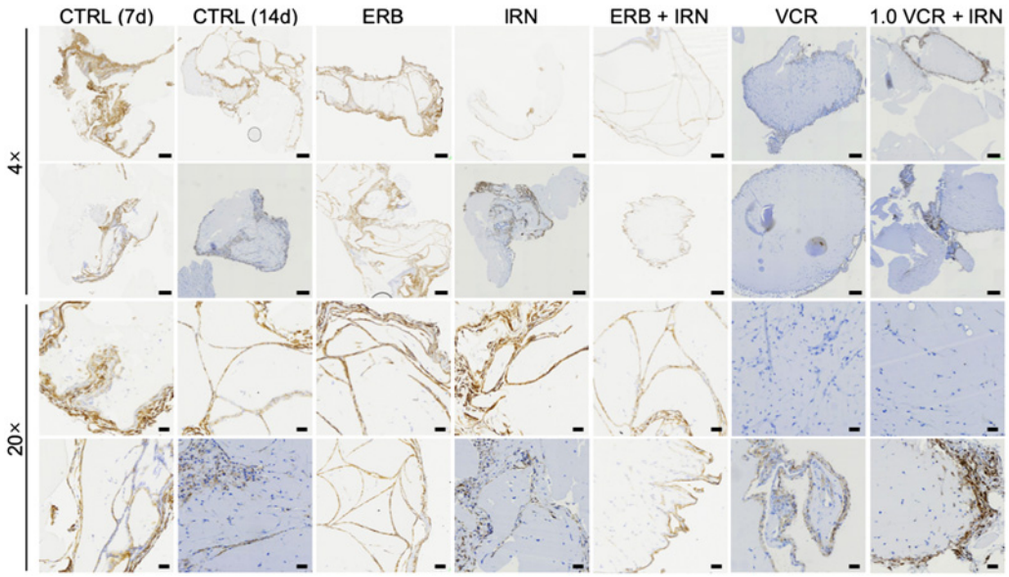

Figure 6.

Eribulin modifies vasculature in subcutaneous Matrigel plugs. Representative images of IHC for CD34 in Matrigel plugs infused with 100 ng/mL VEGF. Matrigel was bilaterally injected subcutaneously into the rear flanks of 3 mice per group, then vasculature was allowed to form for 7 days (represented by CTRL 7d). Mice were then left untreated (CTRL 14d) or treated for 7 days with one cycle of eribulin (ERB), irinotecan (IRN), vincristine (VCR), eribulin + irinotecan (ERB + IRN), or 1.0 mg/kg vincristine + irinotecan (1.0 VCR + IRN); black scale bars = 300 μm for 4× images and 60 μm for 20× images.

also observed with the combination of 0.5 mg/kg vincristine and irinotecan at 24 and 144 hours. With the combination of 1.0 mg/kg vincristine and irinotecan, we detected a decrease in CD34 staining at 24 hours, but approximately twice the amount of CD34 after 144 hours of treatment (**Fig. 5B**). In addition, we assessed the effects of vincristine and irinotecan on α-SMA abundance in ES-4 xenografts. After 24 hours of treatment, we did not observe any significant changes in α-SMA abundance compared with control tumors for any of the treatment groups. After 144 hours, the vincristine and vincristine + irinotecan groups showed increased α-SMA abundance compared with control tumors, but these increases were not statistically significant.

To assess the tumor-independent effects of these treatments on vasculature, we implanted Matrigel plugs containing 100 ng/mL VEGF into C.B.17SC *scid*$^{-/-}$ female mice, allowed vasculature to form for 1 week and then treated the mice with one cycle of eribulin, vincristine, irinotecan, eribulin + irinotecan, or 1.0 mg/kg vincristine + irinotecan. At 1 week after Matrigel implantation, there was clear vascular formation and CD34 positivity (**Fig. 6**). At day 14, plugs from control, eribulin, irinotecan, and eribulin + irinotecan-treated mice showed detectable levels of CD34 in the interior of the Matrigel plugs, whereas plugs from vincristine and vincristine + irinotecan-treated mice only showed detectable CD34 around the plug peripheries (**Fig. 6**), suggesting that vincristine reduced infiltration of vasculature into the Matrigel plugs. The CD34^{+} vasculature from eribulin and eribulin + irinotecan-treated mice appeared to infiltrate the Matrigel plugs to a greater extent and had a smaller diameter than those from the other treatment groups, suggesting that eribulin treatment does not disrupt vasculature to the same extent as vincristine. All plugs showed minimal staining for α-SMA, with plugs from eribulin-treated mice displaying the highest levels (Supplementary Fig. S6).

Discussion

Vincristine plays an essential role in treatment of pediatric solid tumors and acute leukemias, but is associated with significant peripheral neuropathy when administered over prolonged periods. Potentially, substitution of eribulin for vincristine could reduce peripheral neuropathy in patients, hence improve patient quality of life. At the dose levels and schedules of eribulin and irinotecan tested, there is additive or greater than additive activity for the models evaluable. The combination of eribulin–irinotecan was significantly more active than was vincristine–irinotecan in 6 of the 12 models tested, with the vincristine–irinotecan combination being significantly more active for a single model and with three models not being evaluable for time to event comparisons because of the very high activity for each combination. These results reflect in part the ability to combine eribulin with irinotecan at full-dose, whereas vincristine had to be dose-reduced for the combination. However, clinically, combination of vincristine with irinotecan does not require dose reduction of either agent.

For four models, where the EFS was far greater for the eribulin combination compared with the vincristine combination (EFS_{EI}:EFS_{VI} >1.5), each of these models is*TP53* wild type, whereas four of five xenograft models where the combinations had similar activity have mutant *TP53*, the exception being RBD1 in which *TP53* genotype has not been determined. Further, the antitumor activity of the combination correlated with activation of the TP53 pathway as determined by RNA-seq. Notably, the predominant changes in expression were determined by irinotecan treatment. Sestrins 1 and 2 (SESN1/2), induced downstream of DNA-damage-induced TP53, suggest that irinotecan may suppress TORC1 activity (44), that could affect DNA damage repair (45). Also, TP53 apoptosis inducing protein 1 (*TP53AIP1*) was enhanced 40-fold at 24 hours after irinotecan and

almost 80-fold at 144 hours following the eribulin–irinotecan combination. In contrast, eribulin did not induce *TP53AIP1* and only slightly reduced Sestrins 1/2.

The mechanism of action of the eribulin–irinotecan combination appears complex. In tumors, irinotecan prevents eribulin-induced mitotic accumulation, and eribulin appears to reduce biomarkers of DNA damage induced by irinotecan. Thus, from the perspective of mechanism-related biomarkers, the combination appears antagonistic. Similarly, markers of apoptosis tended to be lower in tumors from mice that received either eribulin or vincristine combined with irinotecan, compared with tumors from mice that received single-agent therapy. The reason for this remains obscure, although more rapid induction of apoptosis, may have occurred prior to the later time point (144 hours) when tumors were sampled. An alternative explanation would be that another mechanism of cell death, other than apoptosis, was induced by combination treatments. *In vitro* isobologram analysis indicated antagonism between eribulin and SN-38 whereas there was synergy when SN-38 was combined with vincristine. In contrast, analysis using the CI approach showed little interaction between eribulin and SN-38, thus further studies with additional cell lines will be required to determine whether there is an interaction between these agents *in vitro*.

Giannakakou and colleagues showed that vincristine and paclitaxel enhance TP53 induction in response to doxorubicin (46), and increase TP53 nuclear accumulation. In both ES-4 and KT-11 xenografts, nuclear TP53 was dramatically increased at 24 hours in tumors from combination treated mice, consistent with the onset of caspase 3 cleavage. These results strongly implicate the role of TP53 in mediating the response to eribulin–irinotecan therapy, and support the model proposed whereby inhibition of microtubule dynamics leads to accumulation of nuclear TP53 under conditions of DNA damage. Eribulin would also be anticipated to block trafficking of DNA repair proteins (47), including DNA-PK. As phosphorylation of H2A.X (γ-H2A.X) is partly dependent on the activity of DNA-PK (48), this may account for the decreased γ-H2A.X signal, although in the study by Poruchynsky and colleagues (47), γ-H2A.X was enhanced by microtubule inhibitors.

The antagonism of cytotoxicity *in vitro*, at least by isobologram analysis, suggests the antitumor effects of the combination may be mediated by drug effects on tumor microenvironment, consistent with reports where eribulin induced vascular remodeling and reversed epithelial-to-mesenchymal transition in breast cancer models (21, 23). In addition, eribulin was shown to increase tumor uptake of radiolabeled liposomes (43), possibly due to its effects on tumor vasculature. The greatest increase in tumor CD34 or αSMA positivity occurred at 144 hours in combination-treated tumors (both eribulin and vincristine at the higher dose level), suggesting that combination treatment increased vascularity. In contrast, irinotecan appeared toxic to vascular cells that had invaded Matrigel plugs, whereas combination of eribulin and irinotecan was not. Of interest was the observation that in mice treated with eribulin–irinotecan, vascular cells had invaded the plugs whereas in vincristine–irinotecan treated mice vascular cells were abundant at the periphery of the Matrigel plug, but had not invaded. Although further studies are necessary, the results could indicate that vasculature may be maintained in combination-treated tumors, whereas it is destroyed in tumors treated with irinotecan, thus preserving drug delivery when the combination treatment was administered. Further studies will be required to resolve the role of microenvironment in the antitumor activity of the eribulin–irinotecan combination, particularly with respect to the *TP53* status which associates with enhanced tumor response to this combination.

In summary, the combination of eribulin–irinotecan was highly active in most xenograft models of pediatric solid tumors. Several lines of evidence indicate that the combination activates the TP53 pathway and increases nuclear TP53; further, in tumors for which eribulin–irinotecan had greater activity than vincristine–irinotecan, tumors were wild type for *TP53*. Thus, *TP53* status could affect tumor responsiveness to this combination and should be considered in the design of clinical trials.

Disclosure of Potential Conflicts of Interest

No potential conflicts of interest were disclosed.

Authors' Contributions

Conception and design: A.J. Robles, M.A. Smith, P.J. Houghton
Development of methodology: A.J. Robles, A. Bandyopadhyay, S.W. Erickson, M.A. Smith, P.J. Houghton
Acquisition of data (provided animals, acquired and managed patients, provided facilities, etc.): A.J. Robles, R.T. Kurmasheva, Z. Lai
Analysis and interpretation of data (e.g., statistical analysis, biostatistics, computational analysis): A.J. Robles, S.W. Erickson, D. Kurmashev, Y. Chen, P.J. Houghton
Writing, review, and/or revision of the manuscript: A.J. Robles, R.T. Kurmasheva, S.W. Erickson, M.A. Smith, P.J. Houghton
Administrative, technical, or material support (i.e., reporting or organizing data, constructing databases): D.A. Phelps, Y. Chen, P.J. Houghton
Study supervision: P.J. Houghton

Acknowledgments

This work was supported by UO1CA199297 and CA165995 from the NCI. A.J. Robles was supported by the Cancer Prevention and Research Institute of Texas-funded UT Health San Antonio Cancer Biology Training Program (CPRIT; RP170345) and T32CA148724 (NCI). The authors acknowledge the contributions of Edward Favours, Vanessa Del Pozo, Samson Ghilu, and Kathryn Bondra for conducting the *in vivo* studies, and Daniel Robledo for IHC processing.

The costs of publication of this article were defrayed in part by the payment of page charges. This article must therefore be hereby marked *advertisement* in accordance with 18 U.S.C. Section 1734 solely to indicate this fact.

Received June 14, 2019; revised January 13, 2020; accepted March 12, 2020; published first March 17, 2020.

References

1. Jemal A, Ward EM, Johnson CJ, Cronin KA, Ma J, Ryerson B, et al. Annual report to the nation on the status of cancer, 1975-2014, featuring survival. J Natl Cancer Inst 2017;109:djx030.
2. Siegel RL, Miller KD, Jemal A. Cancer statistics, 2018. CA Cancer J Clin 2018;68:7–30.
3. Eissa HM, Lu L, Baassiri M, Bhakta N, Ehrhardt MJ, Triplett BM, et al. Chronic disease burden and frailty in survivors of childhood HSCT: a report from the St. Jude Lifetime Cohort Study. Blood Adv 2017;1:2243–6.
4. Turcotte LM, Neglia JP, Reulen RC, Ronckers CM, van Leeuwen FE, Morton LM, et al. Risk, risk factors, and surveillance of subsequent malignant neoplasms in survivors of childhood cancer: a review. J Clin Oncol 2018;36:2145–52.
5. Henderson TO, Oeffinger KC. Paediatrics: addressing the health burden of childhood cancer survivors—improvements are needed. Nat Rev Clin Oncol 2018;15:137–8.
6. Houghton PJ, Cheshire PJ, Hallman JC, Bissery MC, Mathieu-Boue A, Houghton JA. Therapeutic efficacy of the topoisomerase I

inhibitor 7-ethyl-10-(4-[1-piperidino]-1-piperidino)-carbonyloxy-camptothecin against human tumor xenografts: lack of cross-resistance in vivo in tumors with acquired resistance to the topoisomerase I inhibitor 9-dimethylaminomethyl-10-hydroxycamptothecin. Cancer Res 1993;53:2823–9.
7. Houghton PJ, Cheshire PJ, Hallman JD, 2nd, Lutz L, Friedman HS, Danks MK, et al. Efficacy of topoisomerase I inhibitors, topotecan and irinotecan, administered at low dose levels in protracted schedules to mice bearing xenografts of human tumors. Cancer Chemother Pharmacol 1995;36:393–403.
8. Houghton PJ, Cheshire PJ, Myers L, Stewart CF, Synold TW, Houghton JA. Evaluation of 9-dimethylaminomethyl-10-hydroxycamptothecin against xenografts derived from adult and childhood solid tumors. Cancer Chemother Pharmacol 1992;31:229–39.
9. Peterson JK, Houghton PJ. Drug discovery in pediatric bone and soft tissue sarcomas using in vivo models. In Pappo, A, editor. Pediatric bone and soft tissue sarcomas. Berlin, Heidelberg: Springer; 2006. p. 89–101.
10. Thompson J, George EO, Poquette CA, Cheshire PJ, Richmond LB, de Graaf SS, et al. Synergy of topotecan in combination with vincristine for treatment of pediatric solid tumor xenografts. Clin Cancer Res 1999;5:3617–31.
11. Houghton PJ, Morton CL, Gorlick R, Lock RB, Carol H, Reynolds CP, et al. Stage 2 combination testing of rapamycin with cytotoxic agents by the Pediatric Preclinical Testing Program. Mol Cancer Ther 2010;9:101–12.
12. Houghton PJ, Stewart CF, Cheshire PJ, Richmond LB, Kirstein MN, Poquette CA, et al. Antitumor activity of temozolomide combined with irinotecan is partly independent of O6-methylguanine-DNA methyltransferase and mismatch repair phenotypes in xenograft models. Clin Cancer Res 2000;6:4110–8.
13. Wagner LM, McAllister N, Goldsby RE, Rausen AR, McNall-Knapp RY, McCarville MB, et al. Temozolomide and intravenous irinotecan for treatment of advanced Ewing sarcoma. Pediatr Blood Cancer 2007;48:132–9.
14. Pappo AS, Lyden E, Breitfeld P, Donaldson SS, Wiener E, Parham D, et al. Two consecutive phase II window trials of irinotecan alone or in combination with vincristine for the treatment of metastatic rhabdomyosarcoma: the children's oncology group. J Clin Oncol 2007;25:362–9.
15. Daw NC, Anderson JR, Hoffer FA, Geller JI, Kalapurakal JA, Perlman EJ. A phase 2 study of vincristine and irinotecan in metastatic diffuse anaplastic wilms tumor: results from the children's oncology group AREN0321 study. J Clin Oncology 2014;32:10032.
16. Kawano S, Asano M, Adachi Y, Matsui J. Antimitotic and non-mitotic effects of eribulin mesilate in soft tissue sarcoma. Anticancer Res 2016;36:1553–61.
17. Hirata Y, Uemura D. [Toxic compounds of Palythoa tuberculosa (Coelenterata), palytoxin and its analogs]. Yakugaku Zasshi 1985;105:1–10.
18. Jordan MA, Kamath K, Manna T, Okouneva T, Miller HP, Davis C, et al. The primary antimitotic mechanism of action of the synthetic halichondrin E7389 is suppression of microtubule growth. Mol Cancer Ther 2005;4:1086–95.
19. Smith JA, Wilson L, Azarenko O, Zhu X, Lewis BM, Littlefield BA, et al. Eribulin binds at microtubule ends to a single site on tubulin to suppress dynamic instability. Biochemistry 2010;49:1331–7.
20. Dybdal-Hargreaves NF, Risinger AL, Mooberry SL. Eribulin mesylate: mechanism of action of a unique microtubule-targeting agent. Clin Cancer Res 2015;21:2445–52.
21. Funahashi Y, Okamoto K, Adachi Y, Semba T, Uesugi M, Ozawa Y, et al. Eribulin mesylate reduces tumor microenvironment abnormality by vascular remodeling in preclinical human breast cancer models. Cancer Sci 2014;105:1334–42.
22. Suzuki H, Hirata Y, Suzuki N, Ihara S, Sakitani K, Kobayashi Y, et al. Characterization of a new small bowel adenocarcinoma cell line and screening of anti-cancer drug against small bowel adenocarcinoma. Am J Pathol 2015;185:550–62.
23. Yoshida T, Ozawa Y, Kimura T, Sato Y, Kuznetsov G, Xu S, et al. Eribulin mesilate suppresses experimental metastasis of breast cancer cells by reversing phenotype from epithelial-mesenchymal transition (EMT) to mesenchymal-epithelial transition (MET) states. Br J Cancer 2014;110:1497–505.
24. Kolb EA, Gorlick R, Reynolds CP, Kang MH, Carol H, Lock R, et al. Initial testing (stage 1) of eribulin, a novel tubulin binding agent, by the pediatric preclinical testing program. Pediatr Blood Cancer 2013;60:1325–32.
25. Geier B, Kurmashev D, Kurmasheva RT, Houghton PJ. Preclinical Childhood Sarcoma Models: Drug Efficacy Biomarker Identification and Validation. Front Oncol 2015;5:193.
26. Schafer ES, Rau RE, Berg S, Liu X, Minard CG, D'Adamo D, et al. A phase 1 study of eribulin mesylate (E7389), a novel microtubule-targeting chemotherapeutic agent, in children with refractory or recurrent solid tumors: a children's oncology group phase 1 consortium study (ADVL1314). Pediatr Blood Cancer 2018;65:e27066.
27. Cortes J, O'Shaughnessy J, Loesch D, Blum JL, Vahdat LT, Petrakova K, et al. Eribulin monotherapy versus treatment of physician's choice in patients with metastatic breast cancer (EMBRACE): a phase 3 open-label randomised study. Lancet 2011;377:914–23.
28. Thomas C, Movva S. Eribulin in the management of inoperable soft-tissue sarcoma: patient selection and survival. Onco Targets Ther 2016;9:5619–27.
29. Wozniak KM, Nomoto K, Lapidus RG, Wu Y, Carozzi V, Cavaletti G, et al. Comparison of neuropathy-inducing effects of eribulin mesylate, paclitaxel, and ixabepilone in mice. Cancer Res 2011;71:3952–62.
30. Cigler T, Vahdat LT. Eribulin mesylate for the treatment of breast cancer. Expert Opin Pharmacother 2010;11:1587–93.
31. Houghton PJ, Morton CL, Tucker C, Payne D, Favours E, Cole C, et al. The pediatric preclinical testing program: description of models and early testing results. Pediatr Blood Cancer 2007;49:928–40.
32. Rose WC, Wild R.Therapeutic synergy of oral taxane BMS-275183 and cetuximab versus human tumor xenografts. Clin Cancer Res 2004;10:7413–7.
33. Trapnell C, Roberts A, Goff L, Pertea G, Kim D, Kelley DR, et al. Differential gene and transcript expression analysis of RNA-seq experiments with TopHat and Cufflinks. Nat Protoc 2012;7:562–78.
34. Anders S, Pyl PT, Huber W. HTSeq—a Python framework to work with high-throughput sequencing data. Bioinformatics 2015;31:166–9.
35. Anders S, Huber W. Differential expression analysis for sequence count data. Genome Biol 2010;11:R106.
36. Subramanian A, Tamayo P, Mootha VK, Mukherjee S, Ebert BL, Gillette MA, et al. Gene set enrichment analysis: a knowledge-based approach for interpreting genome-wide expression profiles. Proc Natl Acad Sci U S A 2005;102:15545–50.
37. Morgan RJ, Synold TW, Longmate JA, Quinn DI, Gandara D, Lenz HJ, et al. Pharmacodynamics (PD) and pharmacokinetics (PK) of E7389 (eribulin, halichondrin B analog) during a phase I trial in patients with advanced solid tumors: a California Cancer Consortium trial. Cancer Chemother Pharmacol 2015;76:897–907.
38. Stewart CF, Zamboni WC, Crom WR, Houghton PJ. Disposition of irinotecan and SN-38 following oral and intravenous irinotecan dosing in mice. Cancer Chemother Pharmacol 1997;40:259–65.
39. Crom WR, de Graaf SS N, Synold T, Uges DRA, Bloemhof H, Rivera G, et al. Pharmacokinetics of vincristine in children and adolescents with acute lymphocytic leukemia. J. Pediatr., 1994;125:642–649.
40. Carol H, Boehm I, Reynolds CP, Kang MH, Maris JM, Morton CL, et al. Efficacy and pharmacokinetic/pharmacodynamic evaluation of the Aurora kinase A inhibitor MLN8237 against preclinical models of pediatric cancer. Cancer Chemother Pharmacol 2011;68:1291–304.
41. Kuznetsov G, Towle MJ, Cheng H, Kawamura T, TenDyke K, Liu D, et al. Induction of morphological and biochemical apoptosis following prolonged mitotic blockage by halichondrin B macrocyclic ketone analog E7389. Cancer Res 2004;64:5760–6.
42. Kuleshov MV, Jones MR, Rouillard AD, Fernandez NF, Duan Q, Wang Z, et al. Enrichr: a comprehensive gene set enrichment analysis web server 2016 update. Nucleic Acids Res 2016;44:W90–7.
43. Ito K, Hamamichi S, Abe T, Akagi T, Shirota H, Kawano S, et al. Antitumor effects of eribulin depend on modulation of the tumor microenvironment by vascular remodeling in mouse models. Cancer Sci 2017;108:2273–80.
44. Budanov AV, Karin M. p53 target genes sestrin1 and sestrin2 connect genotoxic stress and mTOR signaling. Cell 2008;134:451–60.
45. Shen C, Oswald D, Phelps D, Cam H, Pelloski CE, Pang Q, et al. Regulation of FANCD2 by the mTOR pathway contributes to the resistance of cancer cells to DNA double-strand breaks. Cancer Res 2013;73:3393–401.
46. Giannakakou P, Nakano M, Nicolaou KC, O'Brate A, Yu J, Blagosklonny MV, et al. Enhanced microtubule-dependent trafficking and p53 nuclear accumulation by suppression of microtubule dynamics. Proc Natl Acad Sci U S A 2002;99:10855–60.
47. Poruchynsky MS, Komlodi-Pasztor E, Trostel S, Wilkerson J, Regairaz M, Pommier Y, et al. Microtubule-targeting agents augment the toxicity of DNA-damaging agents by disrupting intracellular trafficking of DNA repair proteins. Proc Natl Acad Sci U S A 2015;112:1571–6.
48. Rogakou EP, Pilch DR, Orr AH, Ivanova VS, Bonner WM. DNA double-stranded breaks induce histone H2AX phosphorylation on serine 139. J Biol Chem 1998;273:5858–68.